Chinese Chemical Letters 34 (2023) 107213

Contents lists available at ScienceDirect

Chinese Chemical Letters

journal homepage: www.elsevier.com/locate/cclet

Computational design of BC_3N_2 based single atom catalyst for dramatic activation of inert CO_2 and CH_4 gasses into CH_3COOH with ultralow CH_4 dissociation barrier

Chenxu Zhao[a], Menghui Xi[a], Jinrong Huo[b], Chaozheng He[a,*], Ling Fu[c,*]

[a] Institute of Environment and Energy Catalysis, School of Materials Science and Chemical Engineering, Xi'an Technological University, Xi'an 710021, China
[b] School of Sciences, Xi'an Technological University, Xi'an 710021, China
[c] College of Resources and Environmental Engineering, Tianshui Normal University, Tianshui 741001, China

ARTICLE INFO

Article history:
Received 16 January 2022
Revised 5 February 2022
Accepted 9 February 2022
Available online 14 February 2022

Keywords:
Density functional theory
CO_2/CH_4 coactivation
2D BC_3N_2 substrate
CH_3COOH production

ABSTRACT

The production of CH_3COOH from CO_2 and CH_4 has stimulated much interest due to the high energy density of C2 species. Various kinds of catalysts have been developed while the high dissociation barrier of CH_4 and low selectivity still hinders the efficiency of the reaction. We have herein proposed a novel catalyst with single metals loaded on 2D BC_3N_2 substrate (M@2D-BC_3N_2) based on density functional theory. Among numerous candidates, Pt@2D-BC_3N_2 possesses the most favorable reactivity with an ultralow barrier of CH_4 splitting (0.26 eV), which is due to the efficient capture ability of CH_4 on Pt site. Besides, the selectivity for CH_3COOH is also very high, which mainly stems from the unique electronic properties of molecules and substrate: The degenerated states, including s, p_x, p_y and p_z, in CO_2 reflects the existence of delocalized π bonds between C and O. This can interact with states of Pt(s), Pt(p_z), Pt(d_{xz}), Pt(d_{yz}),and Pt(z^2) in Pt@2D-BC_3N_2. The kinetics model also proves that our system can promote CH_3COOH production *via* simply increasing the temperature or the coverage of CH_4 and CO_2. Our results provide a reasonable illustration in clarifying mechanism and propose promising candidates with high reactivity for further study.

The increased CO_2 level in the atmosphere has caused many damage in climate, such as greenhouse effect. Therefore, the topic on carbon capture and storage has been proposed as a solution. The captured CO_2 has also stimulated the research of CO_2 conversion [1–3]. In the meantime, CH_4 has been treated as an attractive source of hydrogen energy at present and can be obtained from coal-bed gas in large quantity [4]. The CO_2 conversion with the assistance of CH_4 can realize the synthesis of value-added chemicals such as HCOOH, CH_3COOH, CH_3OH, CO [5]. Among these products, the synthesis of CH_3COOH has been investigated extensively due to the 100% utilization of atoms in CO_2 and CH_4. Besides, CH_3COOH is a fuel with high energy density compared to other C1 products [6–9]. This strategy can alleviate human's dependence on conventional fossil fules and simultaneously reduce the detrimental impact of greenhouse gasses. The most widely studied reaction for simultaneous activation of CO_2 and CH_4 is the production of CO/H_2 syngas [10–15]. However, the study of the coupling of CH_4 and CO_2 to C2 products is still an emerging area. The major challenge of this reaction exists in the simultaneous activation of CH_4 and CO_2, especially the process of CH_4 dissociation into CH_3 and H. These have been extensively studied in our previous works [16–19]. Therefore, it is highly desired to develop novel catalyst with high efficiency. As reported in previous studies, the final products of CO_2~CH_4 co-activation mainly include CH_3COOH and HCOOH. The major intermediate of CH_3COOH production is CH_3COO, which derived from the combination between CH_3 and CO_2. For HCOOH production, there exists two intermediates: COOH and HCOO. In other words, the H atom can bond with CO_2 on both C and O atoms. In pioneering works, direct production of CH_3COOH *via* CO_2 and CH_4 has been carried out on several heterogeneous catalysts, such as Co-Cu metal oxides [7], zeolite based catalysts [20], $(ZnO)_3$-In_2O_3 [21], Pd/C [8], Pt/Al_2O_3 [9], Co-Pd/TiO_2 [22], NiO/NiF [23] and ZnO/r-GO [24]. While, the low conversion efficiency and poor selectivity still hinder the development of catalysts in this direction. The main issue that hinders the reactivity of catalysts exists in the effective adsorption and dissociation of inert CH_4. Wang *et al.* have obtained only −0.04 eV adsorption energy for CH_4 on Co(001) surface, which agrees with the following study of Zhang *et al.* (−0.06 eV) [25,26]. Besides, The activation

* Corresponding authors.
E-mail addresses: hecz2019@xatu.edu.cn (C. He), ful263@nenu.edu.cn (L. Fu).

https://doi.org/10.1016/j.cclet.2022.02.018
1001-8417/

barrier for CH_4 dehydrogenation, $^*CH_4 \rightarrow {}^*CH_3 + {}^*H$, has reached to 0.95 eV in Zhang's study [26]. Deo *et al.* have also revealed the weak van der Waals interaction between CH_4 and Ni based alloys with only ~−0.02 eV adsorption energies [27]. Moreover, the reaction barrier of CH_4 dissociation has reached to 1.78 eV (0.92 eV) for Cu (Ni) [27].

In order to improve the reactivity, many research has also focused on the reaction mechanism. The first step of coupling between CO_2 and CH_4 is CH_4 adsorption and further dehydrogenation to CH_3, which has been extensively studied on metals [21,28-36]. Ge *et al.* have realized the C-H activation in CH_4 *via* introducing M-O pair at oxide-oxide interface [21]. Hu *et al.* has studied the transformation of CH_4 to C and H on Pd(100) surface from the aspect of valencies, which emerges clear relationship with the location of transition states [30]. Kim *et al.* have introduced OH groups onto Ir(110) surface and successfully achieved CH_4 activation at low temperature [37]. Jiao *et al.* has demonstrated that the rate controlling step of CH_4 dissociation is the adsorption process and the key intermediate is CHO on Ni(111) surface [32]. Baroni *et al.* has designed a complex of Rh@Cu(111) as model catalyst, which can hinder the second dehydrogenation step ($CH_3 \rightarrow CH_2 + H$) with respect to the first ($CH_4 \rightarrow CH_3 + H$) [33]. Boukelkoul *et al.* have doped Cu(100) surface with W, which proved to be effective for CH_4 dissociation [38]. Gong *et al.* has studied conversion between CH_4 and CH_3 on both flat and stepped Co(0001) surface and suggested that the reaction is not sensitive to structure [35]. However, to the best of our knowledge, the insertion of CO_2 into the metal-CH_3 site is also essential for CH_3COOH formation. Wang *et al.* has suggested that CO_2 insertion into Cu-CH_3 bond is the most favorable path in the formation of CH_3COOH *via* comprehensive comparison of different pathways [5]. Ge *et al.* has studied the C-C coupling reaction on a Zn-doped ceria catalyst. The results show that the Zn dopant may stabilize the methyl group and further contribute the formation of CH_3COOH from CH_4 and CO_2 [39]. Park *et al.* have indicated that the M^+ cation in the M^{+-}ZSM-5 catalyst can assist the activation of CO_2 and subsequent reaction with CH_3 [40]. However, the origin of reactivity still remains elusive. Besides, the mechanism of the interaction between adsorbed molecules and catalyst need to be revealed in more details in current studies.

In our previous study, we have successfully predicted a two dimensional BC_3N_2 (2D BC_3B_2) substrate. This structure is like graphene with B, C and N atoms bonded together upon sp^2 hybridization. Compared with graphene, boron nitride and other graphene materials, each hexagonal primitive unit cell of the BC_3N_2 has one more electron than them. Such a multi-electron system may be beneficial to catalysis due to its advantages in electron transfer rate and effective mass, which is beneficial than other B/C substrates like B_2C [5,41-44].

Inspired by the pioneering works, we attempted to design a novel 2D BC_3N_2 based catalyst with single metals loaded on it (M@2D-BC_3N_2) and calculated properties *via* density functional theory. Among these candidates, Pt@2D-BC_3N_2 is the most promising catalyst to realize effective activation of CH_4 and CO_2 with ultralow barriers for CH_4 splitting (0.26 eV) and CO_2~CH_3 combination (0.86 eV). The selectivity for CH_3COOH is also very high, which mainly stems from the unique electronic properties of molecules and substrate: The delocalized π bonds in CO_2, caused by degenerated states of s, p_x, p_y and p_z between C and O, can interact dramatically with states of Pt(s), Pt(p_z), Pt(d_{xz}), Pt(d_{yz}) and Pt(z^2) in Pt@2D-BC_3N_2. The kinetics model also proves that our system can promote CH_3COOH production *via* simply increasing the temperature or the coverage of CH_4 and CO_2. Our results provide a reasonable illustration in clarifying mechanism and propose promising candidates with high reactivity for further study.

All the first-principles spin-polarized calculations were performed by using the Vienna ab initio simulation package (VASP) [45,46]. The ion-electron interactions were described by the projector augmented wave method [47]. The generalized gradient approximation (GGA) is described in the Perdew Burke Ernzerhof form and the cutoff energy for plane-wave basis is set as 400 eV. The convergence criterion for the residual force and energy was set to 0.05 eV/Å and 10^{-5} eV, respectively, during the structure relaxation. And for all calculations, we considered the vander Waals force correction by using MBD approach in the Grimme scheme [48]. Supercells consisting of $3 \times 3 \times 1$ 2D BC_3N_2 unit cells were used and the Brillouin zones were sampled by a Monkhorst-Pack k-point mesh with a $2 \times 2 \times 1$ k-point grid for structure relaxation, while denser k-points mesh of $7 \times 7 \times 1$ were used for electronic property evaluations. The Bader charge analysis was employed for the charge transfer. A vacuum space of 15 Å was employed to avoid the interaction between two periodic units. The above methods have been widely used in pioneering studies especially in catalytic areas [49–81].

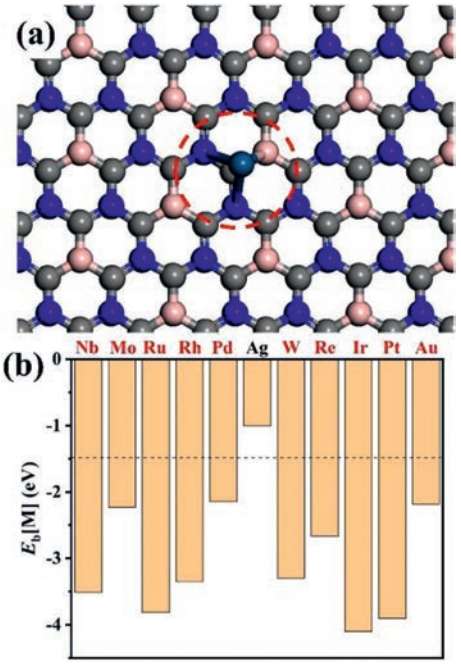

Fig. 1. (a) The configuration of 2D BC_3N_2 with metal atom loaded on it. The atom in the red cycle denotes the doped metal atom. (b) Binding energies of metal atoms on 2D BC_3N_2.

Our predicted 2D BC_3N_2 exhibits a hexagonal network structure (Fig. 1 and Fig. S1 in Supporting information). In 2D BC_3N_2, each unit cell has one more electron, leading to a high electron-transfer rate (more details can be obtained in Ref [30]). This character may be beneficial to activate inert molecules such as CO_2 and CH_4. We thus choose 2D BC_3N_2 as the substrate for single metal atoms to construct a novel catalyst (denoted as M@2D-BC_3N_2) in production of CH_3COOH *via* CO_2 and CH_4.

We first discuss the adsorption sites for single metal atoms loaded on 2D BC_3N_2. To identify the most stable M@2D-BC_3N_2 configurations, metal atoms is placed on various sites above BC_3N_2 (Fig. S1). Each situation is fully relaxed and the most stable structures are confirmed based on systems with the largest binding energies (E_b) for metal atoms on 2D BC_3N_2 as summarized in Table S1 (Supporting information). The binding energies are generally larger than −2 eV except for Ag, indicating the M@2D-BC_3N_2 complex is stable. In other words, the binding strength between 2D-BC_3N_2 and metal atoms is big enough to prohibit the aggregation of single atoms into clusters.

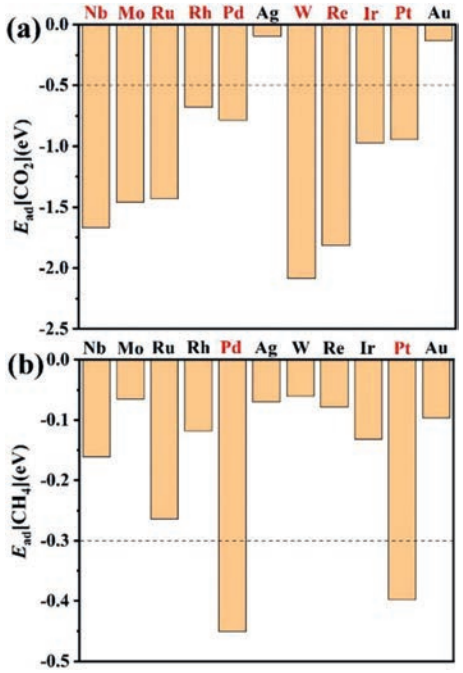

Fig. 2. Adsorption energies for (a) CO_2 and (b) CH_4 on M@2D-BC_3N_2.

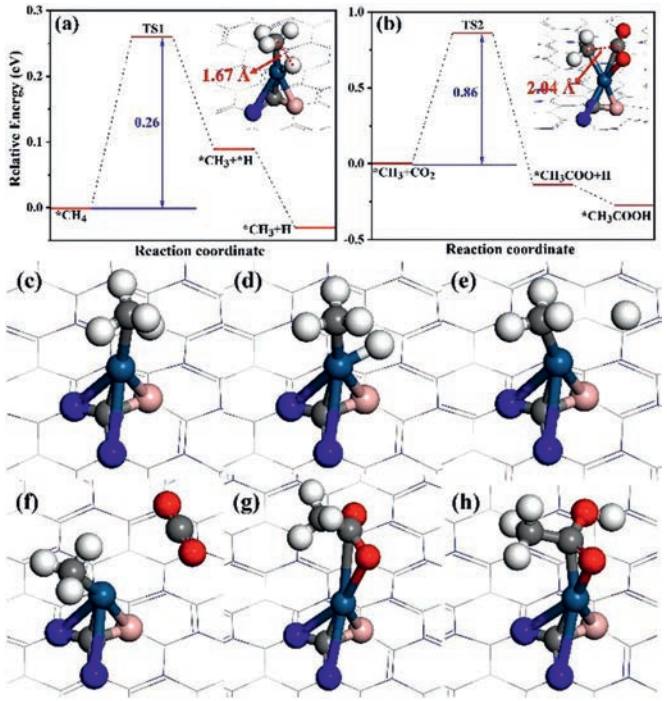

Fig. 3. The reaction pathways of (a) CH_4 dissociation and (b) combination of CO_2 and CH_3. The configurations of transition states are displayed in the insets of (a) and (b). The configurations of (c) $^*CH_4$, (d) $^*CH_3$+$^*H$, (e) $^*CH_3+H$, (f) $^*CH_3+CO_2$, (g) $^*CH_3COO$, and (h) CH_3COOH on Pt@2D-BC_3N_2.

The optimum adsorption configurations of CO_2 are discussed comprehensively with different orientations. This is due to the linear character of CO_2 molecule, which may lead to various adsorption behavior on single-atom sites (Fig. S2 in Supporting information). After calculation of adsorption energies (E_{ad}), the favorable orientation is assumed as the CO_2 molecule adsorbed on metal-atom site with C-O bond pointing to the N atom in the hexagon unit. About the coordination number, CO_2 tends to binds M@2D-BC_3N_2 bidentately with both C and O atoms. Similar conclusions can be obtained in other M@2D-BC_3N_2 systems. The final structures after fully geometric optimization are displayed in Fig. S3 (Supporting information).

As shown in Fig. 2, the adsorption energies for CO_2 are generally larger than −0.5 eV except for Ag and Au, which is remarkably larger than that of CH_4 ($E_{ad}[CH_4]$ are generally lower than −0.3 eV). Therefore, the adsorption process of CH_4 is treated as the rate determined step for simultaneous activation of CO_2 and CH_4. Pt@2D-BC_3N_2 and Pd@2D-BC_3N_2 possess the largest adsorption energy of −0.40 eV and −0.45 eV. However, Pt possesses significant advantages in binding energy on 2D BC_3N_2 than Pd ($E_b[Pt] = -3.91$ eV *vs.* $E_b[Pd] = -2.15$ eV). We thus serve Pt@2D-BC_3N_2 system as the most promising candidate for CH_3COOH production.

In order to determine the accurate reactivity of the reaction, we have performed many analysis such as reaction energy, transition states and frequency. The reaction begins with the adsorption of CH_4 on Pt@2D-BC_3N_2 and further dissociates to $^*CH_3$ and $^*H$. Additional combination between CO_2 and $^*CH_3$ can form $^*CH_3CO_2$ intermediate, which can eventually be hydrogenated into CH_3COOH as final product. For the co-adsorption state of $^*CH_3$ and $^*H$, the $^*H$ can spontaneously separate away from $^*CH_3$ with a negative reaction energy of −0.12 eV. In contrast, CO_2 cannot adsorb together with CH_3 on Pt@2D-BC_3B_2 and combine directly with $^*CH_3$ in gas phase to produce CH_3COO. We first consider the $CH_4 \rightarrow {}^*CH_3 + {}^*H$ step: The catalytic reactivity of CH_4 dehydrogenation is surprisingly high with an ultralow reaction barrier of 0.26 eV (Fig. 3), validating the ability of Pt@2D-BC_3N_2 in activating CH_4. The length of C-H bond in CH_4 is 1.10 Å at initial state and has enlarged into 2.15 Å after dissociation. The configuration of transition state is shown in the inset of Fig. 3 with a C-H bond length of 1.67 Å. The rate determined step (RDS) of $CH_4 + CO_2 \rightarrow CH_3COOH$ reaction is $^*CH_3 + {}^*H + CO_2 \rightarrow CH_3CO_2 + {}^*H$ step with a reaction barrer of 0.86 eV, which can be easily overcome at only 70 °C. The CH_3CO_2 product possesses a C-C bond length of 1.52 Å, which is 2.04 Å in transition states as shown in Fig. 3 and Table S2 (Supporting information). The summarized reaction processes for steps of $CH_4 \rightarrow {}^*CH_3 + {}^*H$ and $^*CH_3 + {}^*H + CO_2 \rightarrow CH_3CO_2 + {}^*H$ are demonstrated in Fig. S4 (Supporting information) and the continuous process for CH_3COOH production is shown in Fig. S5. The only one imaginary frequency of −552.11 cm^{-1} for CH_3∼H (−419.23 cm^{-1} for CH_3∼CO_2) indicates the transition state has been searched correctly for these steps (Table S3 in Supporting information). The results calculated above has illustrated that Pt@2D-BC_3N_2 could be a dramatically efficient catalyst for activation of inert gasses into CH_3COOH.

In addition to CH_3COOH, HCOOH is also an important production that we cannot ignore. The major intermediates for HCOOH production include $^*COOH$ and $^*HCOO$, which derived from the combination between $^*H$ and $^*CO_2$. We thus calculate the reaction barriers of $^*CO_2 + {}^*H \rightarrow {}^*COOH$ and $^*CO_2 + {}^*H \rightarrow {}^*HCOO$. The reaction barriers are 1.51 eV and 1.01 eV for $^*COOH$ and $^*HCOO$ pathways (Figs. S6 and S7 in Supporting information), which are all larger than CH_3COOH production (0.86 eV). This may indicate that HCOOH production may be hindered by $^*CO_2$ hydrodyzation process, leading to the higher selectivity for CH_3COOH comapred to HCOOH. We therefore focuse our study on the CH_3COOH production on Pt@2D-BC_3N_2.

Our designed Pt@2D-BC_3N_2 catayst possesses both notably high adsorption ability and low barrier compared to TM systems. Especially for CH_4 dissociation, this is a general rate controlling step on transition metals (TMs) in pioneering studies as shown in Table 1. The high barriers on TMs (0.92∼1.78 eV) generally resulted from the weak binding strength (−0.02∼−0.04 eV) as the situations on Co, Ni, and Cu. In comparison, Pt exhibits higher CH_4 adsorp-

Table 1
Various reactivity data of CH_4 dissociation including activation barriers (E_a), bond strength of C-H for transition states (d(C-H)), and adsorption energies of CH_4 ($E_{ad}[CH_4]$) for systems of Co, Ni, Cu, Pt, Ir, and our designed Pt@2D-BC_3N_2.

Catalyst	E_a (eV)	d(C-H) (Å)	$E_{ad}[CH_4]$ (eV)
Co(001)	0.95 [26]	1.55 [26]	~−0.04 [25,26]
Ni(111)	0.92 [27]	1.44 [27]	~−0.02 [27]
Cu(111)	1.78 [27]	1.54 [27]	~−0.02 [27]
Pt(111)	0.57 [55]	–	−0.25 [56]
Ir(111)	0.55 [55]	–	–
Pt@2D-BC_3N_2	0.26	1.67	−0.40

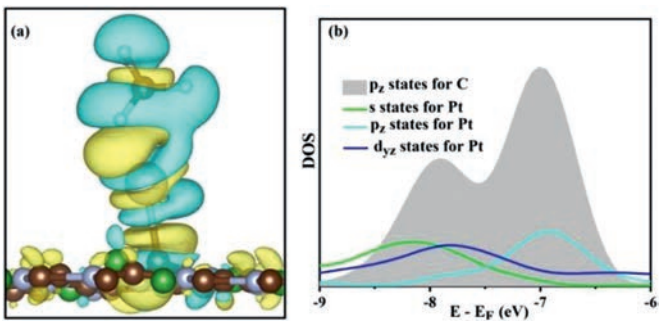

Fig. 4. (a) The charge density difference and (b) density of states (DOS) for hybridization between Pt and C atoms for CH_4 adsorbed on Pt@2D-BC_3N_2. The charge depletion and accumulation were depicted by cyan and yellow, respectively.

tion energy of −0.25 eV, leading to a reduced activation barrier of 0.55 eV. Therefore, the effective capture ability of CH_4 can be treated as the origin for high reactivity of CH_4 splitting. The C-H bond has been enlonged to 1.67 Å, which is much longer than that on transition metals (1.44~1.55 Å). This may illustrate that CH_4 has been sufficiently activated on Pt@2D-BC_3N_2. Thus, the interaction of CH_4 with the substrate can weaken the strength of C-H bond and eventually decrease the dissociation barrier of CH_4.

To clarify the ultrahigh reactivity of Pt@2D-BC_3N_2 in CH_3COOH production, we focus our research on the activation of CO_2 and CH_4 in this part mainly from the hybridizations between various states. For CH_4 adsorption, the charge density difference between CH_4 and Pt@2D-BC_3N_2 demonstrates the dramatic accumulation of electrons between Pt atom and C atom in CH_4, indicating a covalent bond nature (Fig. 4). The density of states (DOS) of Pt and C atoms can reveal the interaction as hybridization between C(p_z), Pt(s), Pt(P_z) and Pt(d_{yz}) states.

For CO_2 adsorption, the interaction of CO_2 molecules with active sites leads to changes in the geometrical properties of CO_2: The angle of O-C-O bond has changed to 117.22° after adsorption, which is in contrast with the value of 180° in free state for CO_2. This may indicate the initial steps of chemical adsorption. As mentioned above, CO_2 tends to bond with Pt atom with both C and O atoms, which possess strongly degenerate between states, including s, p_x, p_y, and p_z. This may indicate the existence of delocalized π bonds in CO_2 as shown in Figs. 5a and b. The degenerate s~p states of O and C will further interact with Pt states, such as s, p_z, d_{yz}, d_{xz} and $d_z{}^2$ (Figs. 5c and d). The overlapping of electronic density regions between Pt site and CO_2 may lead to charge transfer between substrate and adsorbed species (Fig. S9 in Supporting information). The bader charge analysis has shown that Pt@2D-BC_3N_2 has transferred −0.37 e charge to CO_2, leading to a colvalent bond interaction between CO_2 and Pt@2D-BC_3N_2. For the CO_2 adsorbed on Pt@2D-BC_3N_2, the valence state of C (O) atom is about +1.63 (−1) (Fig. S8 in Supporting information). The valence is quantified using bader charge with CO_2 negatively charged with −0.37 e, which is agreed with the situation of Cu. The electrons can move to the lowest unoccupied orbitals of adsorbed CO_2 and

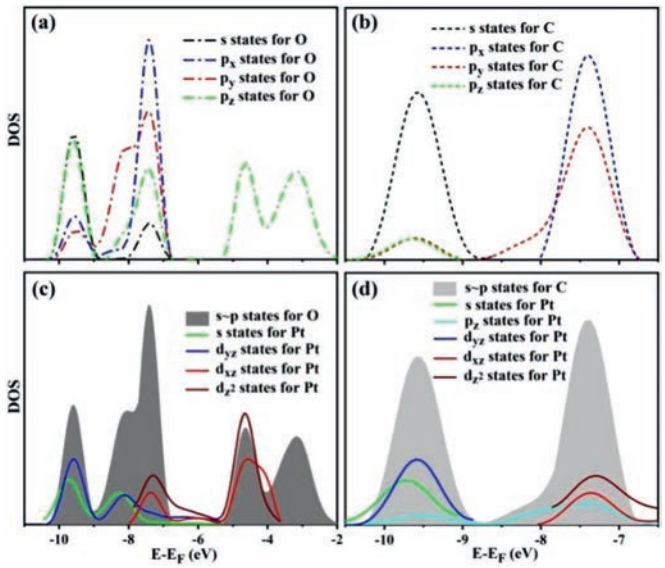

Fig. 5. Density of states (DOS) of degenerate between s and p states in (a) O and (b) C. The DOS in (c) and (d) also exhibit the degenerate states of (c) O and (d) C with s, p and d states in Pt.

Table 2
The rate constant and equilibrium constant of steps under various temperature.

Temperature (K)	350	400	450	500	550	600
K_1	5.95	4.10	3.07	2.44	2.02	1.72
K_2	6.49	11.58	18.17	26.06	35.00	44.75
K	15.83	23.46	31.85	40.67	49.68	58.70

eventually stabilize the systems. The characters described above has comprehensively illustrated that CO_2 has been totally activated on Pt@2D-BC_3N_2. Above all, the high reactivity of Pt@2D-BC_3N_2 mainly stems from the high capture ability of CO_2 and CH_4 molecules. Moreover, Pt is a material with high cost, which may hinder the practical application. Thus, more research works should be done in our further studies to find out proper substitutes based on the theories proposed in this work.

For quantitative analysis, we have calculated the rate constant of CH_4 dissociation and CO_2~CH_3 combination and listed in Table 2. As mentioned above, the barrier of RDS is 0.86 eV, indicating a temperature of 344 K is at least necessary to activate the reaction. We thus investigated the rate constant (k) of $CO_2 + {}^*CH_3 \rightarrow {}^*CH_3COO$ and its related step of CH_4 disscociation at a temperature range of 350~600 K.

The relation between the reaction rate (r) and corresponding k can be described as follows:

$$r_f = k_f \times \prod \theta_i^{v} \quad (1)$$

$$r_b = k_b \times \prod \theta_i^{v} \quad (2)$$

$$k_f = 10_{12} \times A/B \times e^{-\frac{E_b \times N_A}{RT}} \quad (3)$$

$$k_b = 10_{12} \times C/B \times e^{-\frac{E_b \times N_A}{RT}} \quad (4)$$

$$A = \prod f_{ir} \quad (5)$$

$$B = \prod f_{iTS} \quad (6)$$

$$C = \prod f_{ip} \quad (7)$$

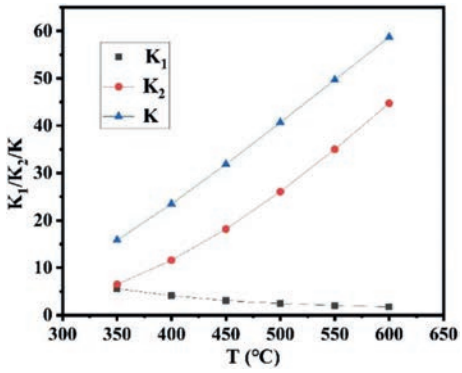

Fig. 6. The correlations between temperature and K_1, K_2 and K.

$$K = k_f/k_b \tag{8}$$

where r_f (r_b) is the reaction rate of forward (backward) reaction; k is the rate constant; θ is the coverage of the adsorbate; A (B, C) is the frequency factor of the reactant (transition state, product); f_r (f_{TS}, f_p) is the frequency of the reactant (transition state, product); K is the equilibrium constant; E_b is the reaction barrier of RCS; N_A is the Avogadro constant. The reaction can reach the equilibrium state at the condition of $r_f = r_b$.

From the formulas above, we can deduce the relationship between K and coverage of CH_4, CO_2 and CH_3COO:

$$\theta[CH_3COO] = K_2 \times \sqrt{K_1} \times \sqrt{\theta[CH_4]} \times \theta[CO_2]$$

$$K = K_2 \times \sqrt{K_1}$$

where K_1 (K_2) is the equilibrium constant of CH_4 dissociation (CO_2~CH_3 combination); K is defined as $K_2 \times \sqrt{K_1}$.

From the data listed in Table 2, we can find that the K_1 (K_2) is (decreased) increased with increasing temperature due to the endothermic (exothermic) reaction character. However, K constantly exhibits increased tendency with increasing temperature. Based on the formula, the production of CH_3COO can be improved *via* increasing the temperature or the coverage of CH_4 and CO_2. This can be attributed to the neglegible change tendency between K_1 and T compared to K_2 situation as shown in Fig. 6. Therefore, K~T exhibits similar tendency as K_2~T.

In conclusion, we have performed density functional theory calculation to study M@2D-BC_3N_2 systems for CH_3COOH synthesis *via* CO_2 and CH_4. We find that Pt@2D-BC_3N_2 can dissociate CH_4 (aggregate CO_2 and CH_3) with an ultralow barrier of 0.26 eV (0.86 eV). The high reactivity and selectivity originate from the high capture ability for CO_2 and CH_4. This phenomenon can be interpreted from the hybridization between various states: The C(p_z) states for CH_4 can interact with states of Pt(s), Pt(p_z) and Pt(d_{yz}) for Pt@2D-BC_3N_2 complex. Besides, the degenerate between states of s, p_x, p_y and p_z in C and O in CO_2 has indicated the delocalized π bonds. This degenerate states can interact with states of Pt(s), Pt(p_z), Pt(d_{xz}), Pt(d_{yz}) and Pt(z^2) for Pt@2D-BC_3N_2. From kinetics aspect, our system can promote CH_3COOH production *via* simply increasing the temperature or the coverage of CH_4 and CO_2. Our study has not only provided clues for catalyst design in CH_3COOH synthesis *via* CO_2 and CH_4, but also enriched the understanding of mechanism in the activation of CO_2 and CH_4.

Declaration of competing interest

The authors declare that they have no known competing financial interests or personal relationships that could have appeared to influence the work reported in this paper.

Acknowledgments

This study was funded by the National Natural Science Foundation of China (No. 21603109), the Henan Joint Fund of the National Natural Science Foundation of China (No. U1404216), the Special Fund of Tianshui Normal University, China (No. CXJ2020-08), the Scientific Research Program Funded by Shaanxi Provincial Education Department (No. 20JK0676). We also appreciate the National Supercomputing Center in Zhengzhou to provide the computational sources

Supplementary materials

Supplementary material associated with this article can be found, in the online version, at doi:10.1016/j.cclet.2022.02.018.

References

[1] W. Wang, S.P. Wang, X.B. Ma, J.L. Gong, Chem. Soc. Rev. 40 (2011) 3703–3727.
[2] M. Aresta, A. Dibenedetto, E. Quaranta, J. Catal. 343 (2016) 2–45.
[3] C. He, R. Wang, D. Xiang, et al., Appl. Surf. Sci. 509 (2020) 145392.
[4] E. McFarland, Science 338 (2012) 340–342.
[5] R. Zhang, L. Song, H. Liu, B. Wang, Appl. Catal. A 443 (2012) 50–58.
[6] P. Tang, Q. Zhu, Z. Wu, D. Ma, Energy Environ. Sci. 7 (2014) 2580–2591.
[7] W. Huang, K.C. Xie, J.P. Wang, et al., J. Catal. 201 (2001) 100–104.
[8] E.M. Wilcox, G.W. Roberts, J.J. Spivey, Catal. Today 88 (2003) 83–90.
[9] J.J. Spivey, E.M. Wilcox, G.W. Roberts, Catal. Commun. 9 (2008) 685–689.
[10] X. Xie, T. Otremba, P. Littlewood, et al., ACS Catal. 3 (2013) 224–229.
[11] L.L. Xu, H.L. Song, L.J. Chou, ACS Catal. 2 (2012) 1331–1342.
[12] M.M. Nair, S. Kaliaguine, F. Kleitz, ACS Catal. 4 (2014) 3837–3846.
[13] A.G. Bhavani, W.Y. Kim, J.S. Lee, ACS Catal. 3 (2013) 1537–1544.
[14] F. Polo-Garzon, D. Pakhare, J.J. Spivey, D.A. Bruce, ACS Catal. 6 (2016) 3826–3833.
[15] K. Yuan, J.-Q. Zhong, X. Zhou, et al., ACS Catal. 6 (2016) 4330–4339.
[16] L. Lin, Z. Shi, J. Huang, et al., Appl. Surf. Sci. 514 (2020) 145900.
[17] L. Lin, J. Huang, W. Yu, et al., Commun. Theor. Phys. 72 (2020) 035501.
[18] L. Fu, R. Wang, C. Zhao, et al., Chem. Eng. J. 414 (2021) 128857.
[19] X. Fu, H. Yang, L. Fu, et al., Chin. Chem. Lett. 32 (2021) 1089–1094.
[20] N. Shahzad, B. Khan, J. Mol. Graph. Model. 105 (2021) 107896.
[21] Y. Zhao, H. Wang, J. Han, et al., ACS Catal. 9 (2019) 3187–3197.
[22] W. Huang, W.Z. Sun, F. Li, Aiche J. 56 (2010) 1279–1284.
[23] J. Li, L. Dou, Y. Gao, et al., J. CO_2 Util. 52 (2021) 101675.
[24] M. Dutra, M. Schmal, R. Guardani, Caltal. Lett. 148 (2018) 3413–3430.
[25] G. Wen, Q. Wang, R. Zhang, et al., Phys. Chem. Chem. Phys. 18 (2016) 27272–27283.
[26] H. Huang, Y. Yu, M. Zhang, Phys. Chem. Chem. Phys. 22 (2020) 27320–27331.
[27] K. Ray, A.S. Sandupatla, G. Deo, Int. J. Quantum Chem. 121 (2021) e26580.
[28] J.M.H. Lo, T. Ziegler, J. Phys. Chem. C 112 (2008) 13642–13649.
[29] W. An, X.C. Zeng, C.H. Turner, J. Chem. Phys. 131 (2009) 174702.
[30] C.J. Zhang, P. Hu, J. Chem. Phys. 116 (2002) 322–327.
[31] A.T. Anghel, D.J. Wales, S.J. Jenkins, D.A. King, Phys. Rev. B 71 (2005) 113410.
[32] S.G. Wang, X.Y. Liao, J. Hu, et al., Surf. Sci. 601 (2007) 1271–1284.
[33] A. Kokalj, N. Bonini, S. de Gironcoli, et al., J. Am. Chem. Soc. 128 (2006) 12448–12454.
[34] J.M. Wei, E. Iglesia, J. Catal. 225 (2004) 116–127.
[35] X.Q. Gong, R. Raval, P. Hu, J. Chem. Phys. 122 (2005) 024711.
[36] G.T. de Jong, D.P. Geerke, A. Diefenbach, F.M. Bickelhaupt, Chem. Phys. 313 (2005) 261–270.
[37] M. Kim, A.D. Franklin, R. Martin, et al., J. Catal. 383 (2020) 181–192.
[38] H. Khettal, M.F. Haroun, M. Boukelkoul, Comput. Theor. Chem. 1186 (2020) 112890.
[39] Y. Zhao, C. Cui, J. Han, et al., J. Am. Chem. Soc. 138 (2016) 10191–10198.
[40] A.M. Rabie, M.A. Betiha, S.-.E. Park, Appl. Catal. B 215 (2017) 50–59.
[41] C. He, R. Wang, H. Yang, et al., Appl. Surf. Sci. 507 (2020) 145076.
[42] J. Yu, C. He, C. Pu, et al., Chin. Chem. Lett. 32 (2021) 3149–3154.
[43] H. Yang, C. He, L. Fu, et al., Chin. Chem. Lett. 32 (2021) 3202–3206.
[44] R. Wang, C. He, W. Chen, et al., Chin. Chem. Lett. 32 (2021) 3821–3824.
[45] G. Kresse, D. Joubert, Phys. Rev. B 59 (1999) 1758–1775.
[46] Furthmuller Kresse, Phys. Rev. B 54 (1996) 11169–11186.
[47] Blochl, Phys. Rev. B 50 (1994) 17953–17979.
[48] L.M. Azofra, D.R. MacFarlane, C.H. Sun, Phys. Chem. Chem. Phys. 18 (2016) 18507–18514.
[49] J.R. Huo, L. Fu, C.X. Zhao, C.Z. He, Chin. Chem. Lett. 32 (2021) 2269–2273.
[50] S. Jian, Z. Tian, J. Hu, et al., Adv. Powder Mater. 1 (2022) 100004.
[51] D.Y. Li, L.L. Liao, H.Q. Zhou, et al., Mater. Today Phys. 16 (2021) 100314.
[52] L. Fu, L. Yan, L. Lin, et al., J. Alloys Compd. 875 (2021) 159907.
[53] X. Chen, W.J. Ong, X. Zhao, et al., J. Energy Chem. 58 (2021) 577–585.
[54] J.Y. Luo, P.P. Han, Z.H. Dan, et al., Rare Metals 40 (2021) 3531–3542.
[55] B. Jackson, J. Chem. Phys. 153 (2020) 034704.
[56] A. Gutierrez-Gonzalez, M.E. Torio, H.F. Busnengo, R.D. Beck, Top. Catal. 62 (2019) 859–873.

[57] Y. Jia, F. Li, K. Fan, L. Sun, Adv. Powder Mater. 1 (2022) 100012.
[58] W. Song, J. Wang, L. Fu, et al., Chin. Chem. Lett. 32 (2021) 3137–3142.
[59] M. Mohebinia, C. Wu, G. Yang, et al., Mater. Today Phys. 16 (2021) 100293.
[60] X. Chen, W.J. Ong, Z. Kong, et al., Sci. Bull. 65 (2020) 45–54.
[61] Y. Sun, Z. Deng, X.-.M. Song, et al., Nano-Micro Lett. 12 (2020) 133.
[62] Y. Wang, M. Batmunkh, H. Mao, et al., Chin. Chem. Lett. 33 (2022) 394–398.
[63] X. Lv, W. Wei, F. Li, et al., Nano Lett. 19 (2019) 6391–6399.
[64] H. Hu, H. Yang, X. Yang, et al., Chin. Chem. Lett. 31 (2020) 3213–3215.
[65] Z. Li, Z. Ma, J. Liang, et al., Mater. Today Phys. 22 (2022) 100586.
[66] G. Zhao, W. Ma, X. Wang, et al., Adv. Powder Mater. 1 (2022) 100008.
[67] X. Lv, W. Wei, B. Huang, et al., Nano Lett. 21 (2021) 1871–1878.
[68] H. Jing, P. Zhu, X. Zheng, et al., Adv. Powder Mater. 1 (2022) 100013.
[69] X.J. Fang, L.P. Ren, F. Li, Z.X. Jiang, Z.G. Wang, Rere Metals 41 (2022) 901–910.
[70] Z.Q. Gao, C.Y. Wang, J.J. Li, et al., Acta Phys. 37 (2021) 2010025.
[71] T.T. Wu, W.J. Fan, Y. Zhang, F.X. Zhang, Mater. Today Phys. 16 (2021) 100310.
[72] F. Rao, G. Zhu, W. Zhang, et al., ACS Catal. 11 (2021) 7735–7749.
[73] F. Rao, G.Q. Zhu, W.B. Zhang, et al., Appl. Catal. B 281 (2021) 119481.
[74] Y.H. Wang, R.Q. Li, H.B. Li, et al., Rare Metals 40 (2021) 1410–1417.
[75] L. Yang, Z. Liu, S. Zhu, et al., Mater. Today Phys. 16 (2021) 100292.
[76] C. Pu, J. Yu, L. Fu, et al., Chin. Chem. Lett. 32 (2021) 1081–1085.
[77] M. Jin, W.H. Yang, X.H. Wang, et al., Rare Metals 40 (2021) 858–864.
[78] S. Li, Y. Wang, J. Liang, et al., Mater. Today Phys. 18 (2021) 100396.
[79] T. Zhang, C.T. Liu, Adv. Powder Mater. 1 (2022) 100014.
[80] Y.Z. Wang, Y.M. Ding, C.H. Zhang, et al., Rare Metals 40 (2021) 2785–2792.
[81] D. Zhou, C. Li, F. Yin, et al., Chin. Chem. Lett. 31 (2020) 2325–2329.